Journal of the European Ceramic Society **15** (1995) 1141–1147

0955-2219(95)00088-7
0955-2219/95/$9.50

Structural and Electrical Properties of Iron Manganite Spinels in Relation with Cationic Distribution

T. Battault, R. Legros & A. Rousset*

Laboratoire de Chimie des Matériaux Inorganiques, URA CNRS 1311, Université Paul Sabatier, 118 route de Narbonne, 31062 Toulouse Cedex, France

(Received 5 December 1994; revised version received 19 May 1995; accepted 22 May 1995)

Abstract

Single-phase iron manganite spinels, $Mn_{3-x}Fe_xO_4$ with $O \leq x \leq 1{\cdot}05$, were prepared by thermal processing of iron–manganese co-precipitated formate precursors. Powder X-ray diffraction (XRD) analysis shows a cubic–tetragonal transition for x = 1·05. *The Mössbauer spectroscopy indicates the presence of only trivalent iron ions in both sites of the spinel structure. The electrical measurements show that these iron manganites have the characteristics of negative temperature coefficient thermistors. Moreover, in these solid solutions, the resistivity* ρ *decreases with increasing of iron content* x. *Correlation of the results obtained by XRD, Mössbauer spectroscopy and electrical measurements permits one to infer the cationic distribution, given by* $Mn^{2+}_{1-y}\ Fe^{3+}_{y}\ (Fe^{3+}_{z}\ Mn^{3+}_{2-x}\ Mn^{2+}_{y})\ O^{2-}_{4}$ *with* x = y + z.

1 Introduction

Results obtained in recent years have led to much progress in the development of high performance negative temperature coefficient (NTC) thermistors[1–4] and particularly thin layer ceramics.[5] Generally, these NTC ceramics are based on Mn-spinels. Since both manganese and iron assume multiple valences in oxide structure, it is possible to elaborate spinels over a continuous range of composition from Mn_3O_4 to Fe_3O_4.[6] Thus, in determining the phase diagram of the solids present in the system $Fe_2O_3 - Mn_2O_3 - O_2$ at equilibrium in air, Wickham[7] described the chemical composition of the mixed oxides of iron and manganese which have the spinel crystal structure and proposed the formula $Fe_{3-x}Mn_xO_{4+\delta}$. The value of δ for most of the spinel compositions is very close to zero, yet relatively large for x equal to zero. Pelton *et al.*,[8] through analysis of the phase equilibrium diagram of the Fe_3O_4–Mn_3O_4 spinel system, obtained information on the thermodynamic properties and inferred the distribution of divalent and trivalent cations between the octahedral and tetrahedral sites.

Until now, many papers have been devoted to manganese ferrite $Fe_{3-x}Mn_xO_4$ with $0 \leq x \leq 1$.[9–14] But studies are rare for iron manganite (excess of manganese) and only for the defined compound Mn_2FeO_4. Thus, measurements of magnetic-moment data enabled Eschenfelder[6] to propose a cationic distribution for this compound $Mn^{2+}(Fe^{2+}Mn^{4+})O^{2-}_4$. Using the Mössbauer technique, Tanaka *et al.*[15] introduced both Fe^{3+} and Fe^{2+} ions in octahedral sites following the distributions $Fe^{3+}_{0{\cdot}09}\ Mn^{2+}_{0{\cdot}91}(Fe^{2+}_{0{\cdot}09}\ Fe^{3+}_{0{\cdot}82}\ Mn^{3+}_{1{\cdot}09})\ O^{2-}_4$. More recently, Kulkarni and Darshane,[16] by Mössbauer investigation of $FeMn_2O_4$, showed the equal distribution of Fe^{3+} ions between tetrahedral and octahedral sites and the absence of Fe^{2+} ions in the lattice. Their conductivity and thermopower measurements led them to express the cation distribution of this compound by the formula $Fe^{3+}_{0{\cdot}5}\ Mn^{2+}_{0{\cdot}5}\ (Fe^{3+}_{0{\cdot}5}\ Mn^{2+}_{0{\cdot}5}\ Mn^{3+}_{1-y}\ Mn^{2+}_{y/2}\ Mn^{4+}_{y/2})O^{2-}_4$.

The approach of Rousset *et al.*[17] is to optimize all the manufacturing and electrical parameters of NTC thermistors by a chemical process to establish correlations between composition, structure and electrical properties, so as to understand and rationalize the conventional process. In this respect, the present work reports our results on the preparation of single-phase iron manganite $Mn_{3-x}Fe_xO_4$ with $0 \leq x \leq 1{\cdot}05$. A cation distribution in the compound defined is proposed that takes account of the results obtained for the complete range of these solid solutions. This method appears to be more relevant than the one that only considers only the defined compound Mn_2FeO_4.

*To whom correspondence should be addressed.

2 Experimental

2.1 Preparation of iron manganite powders

Co-precipitated formate precursors were obtained by the addition of water–ethanol solutions at 25°C from $MCl_2.4H_2O$ (with M = Mn, Fe) and ammonium formate. After 30 min, the precipitates were filtered and washed with water–ethanol solution. The different compositions of formate solid solutions studied, $Fe_y\ Mn_{1-y}\ (O_2CH)_2.\ 2\ H_2O$, are listed in Table 1.

After several thermal decomposition tests on formate precursors, we succeeded in obtaining the desired spinel structure phase directly: $Fe_xMn_{3-x}O_4$ (with $x = 3y$). The conditions applied were: rate of temperature increase 150°C h^{-1}, ageing for 4 h at 1000°C, and quenching in air from 1000°C to room temperature.

2.2 Preparation of ceramic samples

To prepare the ceramics, the spinel powders were mixed with an organic binder and pressed into discs under 400 MPa pressure. The resulting discs were fired at 1180°C in air, with 4 h sintering time, and then quenched in air.

The densification of the ceramics was improved by optimizing the percentage of binder. The highest densification, about 95%, was obtained for a ratio of 40 wt% of binder.

2.3 Measurements

X-ray powder diffraction (XRD) measurements were performed at room temperature using an automatic diffractometer (Siemens D501).

The ^{57}Fe Mössbauer spectra were recorded at room temperature with a spectrometer using a 25 mCi ^{57}Co source in Rh matrix. Absolute velocity calibration was carried out with an Fe foil (25 μm thick); isomer shifts (IS) are reported with reference to Fe. The spectra were computer-fitted using a general Lorentzian routine, and a nonlinear least-squares curve-fitting procedure was employed to obtain the best fit to the experimental data. We used IS and quadrupole splitting (QS) to characterize the species.

Table 1. Composition of the formate precursors $Fe_yMn_{1-y}(O_2CH)_2.2H_20$ and the corresponding iron manganites $Fe_xMn_{3-x}O_4$

y	0	0·04	0·13	0·19	0·26	0·35
x	0	0·12	0·39	0·58	0·78	1·05

To determine the electrical characteristics, the ceramic samples were electroded with silver paint and fired at 850°C. Resistivity measurements, ρ, were taken at (25 ± 0·05)°C using a Philips PM2525 multimeter. A second measurement at 85°C gave us the thermal sensitivity B.

3 Results

3.1 XRD analysis

All $Mn_{3-x}Fe_xO_4$ ($0 \leq x \leq 1{\cdot}05$) solid solutions crystallize with a spinel structure. Figure 1 and Table 2 give the overall results, the variation in the lattice parameters a and c, and the c/a ratio. For $0 \leq x \leq 0{\cdot}78$, XRD powders revealed a single tetragonally distorted cubic symmetry spinel phase. This tetragonal distortion, characterized by the ratio c/a, decrease as a function of increasing iron, x, and disappears for x equal 1·05. For $x = 1{\cdot}05$, $Mn_{1.95}Fe_{1.05}O_4$ crystallized with a cubic single phase.

The same results were observed for the ceramics, see Table 3.

3.2 Mössbauer spectroscopy

The Mössbauer spectra of all iron manganite powders have the same form; Fig. 2 shows the Mössbauer spectrum of $Mn_{2.42}Fe_{0.58}O_4$. All the

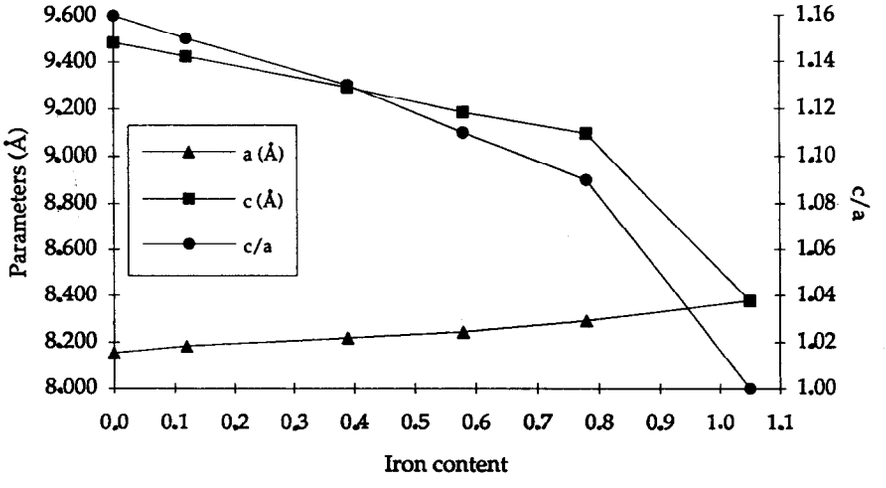

Fig. 1. Variation of the lattice parameters, a and c, and the c/a ratio as a function of iron content.

Table 2. Lattice parameters and *c/a* ratio as a function of iron content, *x*, for the iron manganite powders

x	0	0·12	0·39	0·58	0·78	1·05
a(Å)	8·155	8·183	8·217	8·243	8·291	8·377
c(Å)	9·484	9·423	9·290	9·184	9·096	
c/a	1·16	1·15	1·13	1·11	1·09	1

Table 3. Lattice parameters and *c/a* ratio as a function of iron content, *x*, for the iron manganite ceramics

x	0·12	0·39	0·58	0·78	1·05
a(Å)	8·219	8·215	8·259	8·274	8·341
c(Å)	9·400	9·300	9·181	9·019	
c/a	1·14	1·13	1·11	1·09	1

spectra exhibit two doublets with an isomer shift of between 0·3 and 0·5 mm s^{-1}, indicating the presence of two non-equivalent sites of the Fe^{3+} ion. This could be associated with the presence of Fe^{3+} ions in octahedral and tetrahedral sites. Singh *et al.*[18]

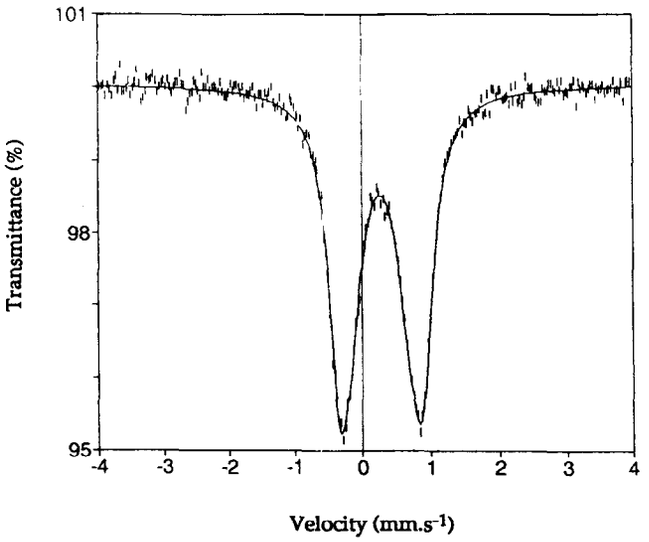

Fig. 2. Mössbauer spectrum of $Mn_{2.42}Fe_{0.58}O_4$.

Table 4. Analysis of the Mössbauer spectra. IS = isomer shift; QS = quadrupole splitting; A = tetrahedral site; B = octahedral site

x	IS_A (mm s^{-1})	IS_B (mm s^{-1})	QS_A (mm s^{-1})	QS_B (mm s^{-1})	% Fe_A^{3+}	% Fe_B^{3+}
0·12	0·369	0·406	1·503	0·978	76·0	24·0
0·39	0·380	0·380	1·336	1·012	57·2	42·8
0·58	0·382	0·372	1·231	0·875	49·9	50·1
0·78	0·383	0·367	1·301	0·891	37·2	62·8
1·05	0.384	0·364	1·297	0·912	21·7	78·3

Table 5. Electrical characteristic data

x	0·39	0·58	0·78	1·05
ρ (Ω cm)	$1{\cdot}431\times10^7$	$0{\cdot}988\times10^7$	$0{\cdot}244\times10^7$	$0{\cdot}202\times10^7$
B (K)	5981	5722	5510	5468

showed that quadrupole splitting is less in octahedral sites than in tetrahedral sites. By quantitative analysis, we can calculate the percentage of Fe^{3+} ions in each site. The percentages are given in Table 4.

3.3 Electrical measurements

Electrical measurements were carried out on the ceramics. Figure 3 shows the variation in dc resistivity, ρ, as a function of iron content, *x*, while Table 5 summarizes the electrical data. The dc resistivity of the composition for $x \leq 0{\cdot}12$ was too high for measurement in our laboratory. For $x > 0{\cdot}12$, resistivity decreased until *x* is equal to 0·78, then remained constant. The substitution of ferric ion in Mn_3O_4, an insulating compound, changed the resistivity from 1 GΩ cm[19] to 2 MΩ cm. The values of thermal sensibility, *B*, also decreased with decreasing resistivity, dropping from 5980 to 5470 K for $0{\cdot}39 \leq x \leq 1{\cdot}05$.

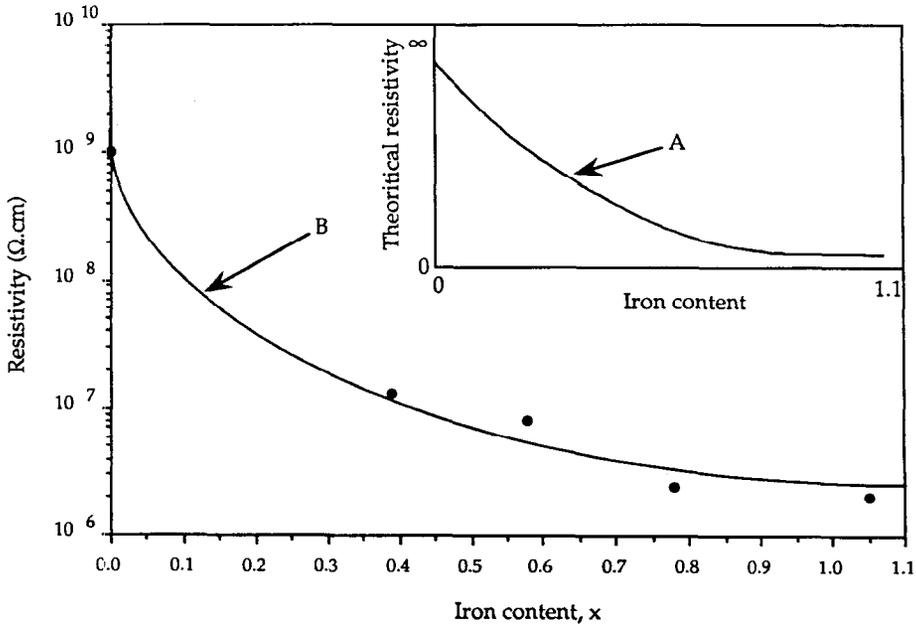

Fig. 3. Variation of resistivity as a function of iron content: (A) theoretical curve and (B) experimental curve.

4 Discussion

4.1 Valency and position of iron cations

Iron manganites were prepared by substituting iron ions for manganese ions in hausmannite Mn_3O_4, the basic crystal structure of manganites. It is now commonly accepted[20,21] that the cation distribution in Mn_3O_4 is Mn^{2+} (Mn_2^{3+}) O_4^{2-}. Thus the iron cation can occupy either the tetrahedral sites (A sites, Mn^{2+} substitution) or octahedral sites (B sites, Mn^{3+} substitution). The Mössbauer results indicate the presence of Fe^{3+} ions only (i.e. no Fe^{2+} ions) located in both octahedral and tetrahedral sites. The introduction of Fe^{3+} ions at octahedral sites does not disturb the overall electrical neutrality of the material, whereas Fe^{3+} in tetrahedral sites does. In the latter case, to preserve electrical neutrality, some Mn^{3+} at B sites change valency to Mn^{2+}. Moreover, the number of Mn^{2+} in octahedral sites is equal to the number of Fe^{3+} in tetrahedral sites. The following ionic configuration can thus be proposed for iron manganites:

$$Mn^{2+}_{1-y}\ Fe^{3+}_{y}\ (Fe^{3+}_{z}\ Mn^{3+}_{2-x}\ Mn^{2+}_{y})\ O^{2-}_{4} \text{ with } x = y + z \quad (I)$$

Using quantitative Mössbauer results, the values of the coefficients x, y and z can be calculated. For example, for $x = 0{\cdot}58$:

$$Mn^{2+}_{0{\cdot}71}Fe^{3+}_{0{\cdot}29}(Fe^{3+}_{0{\cdot}29}\ Mn^{3+}_{1{\cdot}42}\ Mn^{2+}_{0{\cdot}29})\ O^{2-}_{4}$$

The cationic distributions obtained for the other values of x are given in Table 6. Whatever the value of x (total number of iron ions) above 0·12, the number of Fe^{3+} ions in A sites is almost constant, about 0·23 – 0·29, whereas the number of Fe^{3+} ions in B sites increases with the increasing total number of iron ions.

4.2 Cubic–tetragonal transition

Most of the $Mn_{3-x}Fe_xO_4$ solid solutions were found to be tetragonally distorted from cubic symmetry. Hausmannite exhibits a tetragonal distorsion explained by the presence of Mn^{3+} ions in octahedral positions (Jahn–Teller effect). Moreover, Baffier and Huber[22] showed that a minimum concentration of Mn^{3+} ions in octahedral sites is necessary to promote a cooperative Jahn–Taller effect. The minimum is about 50%. Thus a correlation exists between the concentration of Mn^{3+} cations in B sites and the macroscopic distorsion observed by X-ray diffraction. The cationic distribution (I) could explain the decrease in tetragonal distortion as a function of iron content (x) by diminishing the Mn^{3+} ion content in B sites.

Particularly when $x = 1{\cdot}05$, the Mn^{3+} concentration in octahedral sites is below 50% and cubic symmetry appears. These results are in good agreement with the studies of Brabers[23] who pointed out the cubic–tetragonal transition in manganese ferrites $Mn_xFe_{3-x}O_4$ for $x = 1{\cdot}9$, corresponding in this work to iron manganites $Mn_{3-x}Fe_xO_4$ to $x = 1{\cdot}1$.

X-ray diffraction analysis of manganite ceramics revealed the presence of a pure spinel structure. The results concerning the lattice parameters (Table 3) are very close to those observed with spinel powders. Hence we can assume that the ionic distribution of the powder samples does not differ from that of the ceramics.

Table 6. Cationic distributions of the iron manganites $Mn_{3-x}Fe_xO_4$

x	*Cationic distributions*
0	$Mn^{2+}_1(Mn^{3+}_2)O^{2-}_4$
0·12	$Mn^{2+}_{0{\cdot}91}Fe^{3+}_{0{\cdot}09}(Fe^{3+}_{0{\cdot}03}Mn^{3+}_{1{\cdot}88}Mn^{2+}_{0{\cdot}09})O^{2-}_4$
0·39	$Mn^{2+}_{0{\cdot}77}Fe^{3+}_{0{\cdot}23}(Fe^{3+}_{0{\cdot}17}Mn^{3+}_{1{\cdot}60}Mn^{2+}_{0{\cdot}23})O^{2-}_4$
0·58	$Mn^{2+}_{0{\cdot}71}Fe^{3+}_{0{\cdot}29}(Fe^{3+}_{0{\cdot}29}Mn^{3+}_{1{\cdot}42}Mn^{2+}_{0{\cdot}29})O^{2-}_4$
0·78	$Mn^{2+}_{0{\cdot}71}Fe^{3+}_{0{\cdot}29}(Fe^{3+}_{0{\cdot}49}Mn^{3+}_{1{\cdot}22}Mn^{2+}_{0{\cdot}29})O^{2-}_4$
1·05	$Mn^{2+}_{0{\cdot}77}Fe^{3+}_{0{\cdot}23}(Fe^{3+}_{0{\cdot}82}Mn^{3+}_{0{\cdot}95}Mn^{2+}_{0{\cdot}23})O^{2-}_4$

4.3 Electrical properties of ceramics

Electrical conduction in ferrites and manganites is assumed to occur according to the 'hopping' mecanism.[24] It has been determined that hopping will occur if ions of the same element, differing in valency by one unit only, are present in crystallographically equivalent lattice sites.

According to the cationic distribution proposed for iron manganites, formulae I, both Mn^{2+} and Mn^{3+} are present in B sites so that the conditions are correct for electron hopping from Mn^{2+} to Mn^{3+}. The conductivity of the material is determined by the number of ions capable of either donating or accepting electrons in this electron transfer. Thus the electrical conductivity can be written[25]:

$$\sigma = \frac{\sigma_o}{T} NC(1-C) \exp\left(\frac{-E_H}{kT}\right) \text{ with } \sigma'_o = \frac{N_{oct} e^2 d^2 \nu_o}{k}$$

where N_{oct} is a concentration per cm^3 of octahedral sites, d is a jump distance for the charge carrier, ν_o is the lattice vibrational frequency associated with conduction, k is Boltzmann's constant, e the electronic charge, N is a concentration per formulae unit of sites which are available to the charge carriers, C is a fraction of available sites which are occupied by the charge carriers, and E_H is a hopping energy.

The term $NC(1 - C)$ can be rewritten:

$$NC(1-C) = \frac{(Mn^{3+}_{oct})(Mn^{2+}_{oct})}{[(Mn^{3+}_{oct})+(Mn^{2+}_{oct})]^2}$$

Table 7. Comparison between iron manganites and nickel manganites

	Cationic distribution	NC(*1* – C)[a]	d(Å)[b]
$Mn_{2.42}Fe_{0.58}O_4$	$Mn^{2+}_{0.71}Fe^{3+}_{0.29}(Fe^{3+}_{0.29}Mn^{3+}_{1.42}Mn^{2+}_{0.29})O^{2-}_4$	0·141	3·021
$Mn_{2.43}Ni_{0.57}O_4$	$Mn^{2+}_1(Ni^{2+}_{0.57}Mn^{3+}_{0.86}Mn^{4+}_{0.57})O^{2-}_4$	0·240	2·989

$$^{a}NC(1\text{-}C) = \begin{cases} \dfrac{(Mn^{3+}_{oct})\,(Mn^{2+}_{oct})}{[(Mn^{3+}_{oct}) + (Mn^{2+}_{oct})]^2} \\ \text{or} \\ \dfrac{(Mn^{3+}_{oct})\,(Mn^{4+}_{oct})}{[(Mn^{3+}_{oct}) + (Mn^{4+}_{oct})]^2} \end{cases}$$

^{b}d = distance of $\begin{cases} Mn^{2+} - Mn^{3+} \text{ carriers in iron manganites} \\ \text{or} \\ Mn^{3+} - Mn^{4+} \text{ carriers in nickel manganites} \end{cases}$

$$= \begin{cases} \dfrac{a\sqrt{2}}{4} \text{ for cubic phase} \\ \text{or} \\ \dfrac{a'\sqrt{2}}{4} \text{ for tetragonal phase with } a' = \sqrt[3]{a^2c} \text{ (average value)} \end{cases}$$

which represents the probability of finding Mn^{3+} Mn^{2+} pairs in octahedral sites.

As a first approximation, we shall consider only the variation in the last ratio. Thus, the theoretical variation in resistivity can be plotted against iron content and compared with the experimental curve: $\rho = f(x)$. The theoretical variation in resistivity shown in Fig. 3 curve A, calculated for hypothetical configuration I, selected from a previously Mössbauer study, fits well with the experimental data (Fig. 3 curve B). Thus for $0 < x < 0{\cdot}8$, both theoretical and experimental resistivities decrease then remain constant. Table 5 summarizes the electrical data. Note that the substitution of iron ions in hausmannite ($x = 0$) insulating material (resistivity about 10^9 Ω cm) changes the resistivity by only about 10^6 Ω cm. Compared with the substitution of the same number of nickel ions in Mn_3O_4, for example $x = 0{\cdot}57$ nickel ions, the resistivity is about 1650 Ω cm. Two parameters can influence the hopping process: the number and/or the distance of carriers. The higher resistivity in iron manganite can be explained on the one hand by a small number of carriers, 0·141 compared with 0·240 carriers in nickel manganites with approximately the same total number of substituted ions (see Table 7), and, on the other, by the distance of Mn^{2+}–Mn^{3+} carriers in iron manganites (3·021 Å), which is higher than the distance of Mn^{3+}–Mn^{4+} carriers in nickel manganites (2·989 Å).

Figure 4 shows that a plot of log resistivity against the reciprocal of absolute temperature gives a straight-line relationship between these

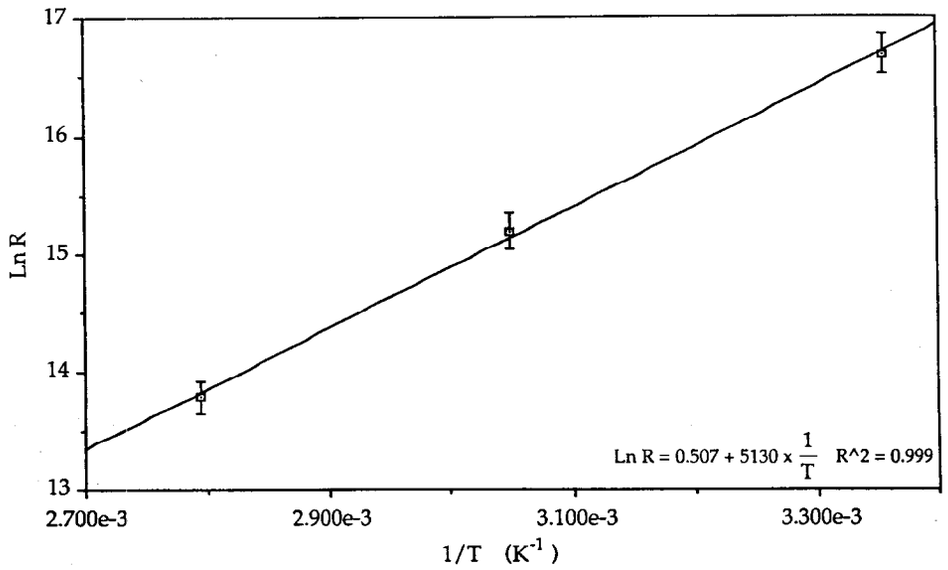

Fig. 4. Variation of ln *R* as a function of inverse of the temperature between 25 and 85°C.

parameters. This result indicates that, in spite of the high resistivity, iron manganites have thermistor characteristics. Moreover, the thermal sensibility is also very high, ranging from 5468 to 5981 K in all solid solutions.

4.4 Cationic distributions

Mössbauer studies indicate that only Fe^{3+} ions are located in both sites of the spinel structure of iron manganites $Mn_{3-x}Fe_xO_4$. Using quantitative results, a cationic distribution is proposed for all solid solutions. In these latter, the number of Mn^{3+} ions in B sites corresponds to the tetragonal distortion, observed by X-ray diffraction, and explains the cubic–tetragonal transition when $x = 1{\cdot}05$.

The electrical resistivity also correlates with the theoretical resistivity calculated by the number of charge carriers from proposed cationic distributions. These results suggest the following ionic distribution model for iron manganite solid solutions:

$$Mn^{2+}_{1-y}\ Fe^{3+}_{y}(Fe^{3+}_{z}\ Mn^{3+}_{2-x}\ Mn^{2+}_{y})\ O^{2-}_{4} \text{ with } x = y + z \quad (1)$$

Differences of opinion exist regarding the distribution and valency states of the cations on the tetrahedral and octahedral sublattices of the spinel structure of iron manganites.[6,15,16] These discrepancies may result from their preparation, since iron manganite are usually prepared by mixtures of oxides. Thus the difficulty of synthesizing single-phase compounds often limits the correlation of structure and properties.

5 Conclusions

Co-precipitated iron–manganese formate was employed to prepare single-phase iron manganite spinels, $Mn_{3-x}Fe_xO_4$ with $0 \leq x \leq 1{\cdot}05$. XRD analysis of these spinels revealed the presence of a single phase having a tetragonally distorted spinel structure for $x < 1{\cdot}05$ and a single cubic spinel phase for $x = 1{\cdot}05$. Mössbauer spectroscopy showed the presence of iron ions in both sites of the spinel structure but only with oxidation degree III. XRD results, combined with Mössbauer spectroscopy, and comparison of experimental and theoretical curves of electrical measurements indicated that the cationic distribution in these spinels approached:

$$Mn^{2+}_{1-y}\ Fe^{3+}_{y}(Fe^{3+}_{z}\ Mn^{3+}_{2-x}\ Mn^{2+}_{y})\ O^{2-}_{4} \text{ with } x = y + z$$

These electro-ceramics display high resistivity and, above all, high thermal sensibility, and should accordingly find interesting industrial applications as NTC thermistors.

References

1. Carnet, R., Etude et développement industriel de céramiques semi-conductrices destinées à la fabrication de thermistances à coefficient de température négatif (CTN) à hautes performances. *Thesis*, University Paul Sabatier, Toulouse, France (1986).
2. Lagrange, A., Caffin, J. P., Fau, P., Legros, R., Metz, R. & Rousset, A., Composition pour thermistances à coefficient de température négatif et de très faible résistivité électrique. *French Patent 8912890* (3 October 1989).
3. Feltz, A., Töpfer, J. & Schirrmeister, F., Conductivity data and preparation route for $NiMn_2O_4$ thermistor ceramics. *J. Eur. Ceram. Soc.*, **9** (1992) 187–91.
4. Martinez Sarrion, M. L. & Morales Sanchez, M., Preparation and characterization of thermistors with negative temperature coefficient, $Ni_xMn_{3-x}O_4$ ($1 \geq x \geq 0{\cdot}56$), from formate precursors. *J. Mater. Chem.*, **3** (1993) 273–7.
5. Lindner, F. & Feltz, A., Thin layer NTC semiconductor ceramics based on $NiMn_2O_4$ and $Zn_zNiMn_{2-z}O_4$ (z = 1/3,2/3). *J. Eur. Ceram. Soc.*, **11** (1993) 269–74.
6. Eschenfelder, A.H., Ionic valences in manganese–iron spinels. *J. Appl. Phys.*, **29** (1958) 378–80.
7. Wickham, D. G., The chemical composition of spinels in the system Fe_3O_4–Mn_3O_4. *J. Inorg. Nucl. Chem.*, **31** (1969) 313–20.
8. Pelton, A. D., Schmalzried, H. & Sticher, J., Thermodynamics of Mn_3O_4–Co_3O_4, Fe_3O_4–Mn_3O_4 and Fe_3O_4–Co_3O_4 spinels by phase diagram analysis. *Ber. Bunsenges. Phys. Chem.*, **83** (1979) 241–52.
9. Tsuji, T., Asakura, Y., Yamashita, T. & Naito, K., Phase equilibria of the Mn–Fe–O system (Fe/Mn = 2). *Solid State Chem.*, **50** (1983) 273–80.
10. Tailhades, Ph., El Guendouzi, M., Rousset, A. & Gillot, B., Sur le comportement des ions du manganèse lors de l'oxydation de magnétites substituées finement divisées., *C. R. Acad. Sci. Paris*, **299** (1986) 13–16.
11. Gillot, B., El Guendouzi, M., Tailhades, Ph. & Rousset, A., Oxidation mechanism of manganese substituted magnetites. *Reactivity of Solids*, **1** (1986) 139–52.
12. Tailhades, Ph., Rousset, A., Bendaoud, R., Fert, A. R. & Gillot, B., Structural study of new defect manganese ferrites. *Mater. Chem. Phys.*, **17** (1987) 521–9.
13. Kolk, B., Albers, A., Hearne, G. R. & Le Roux, H., Evidence of a new structural phase of manganese–iron oxide. *Hyperfine Interactions*, **42** (1988) 1051–4.
14. Jimenez Mateos, J. M., Jones, W., Morales, J. & Tirado, J. L., Composition and cation-valency distribution of cation-deficient Mn/Fe spinel oxides. *J. Solid State Chem.*, **93** (1991) 443–53.
15. Tanaka, M., Mizoguchi, T. & Aiyama, Y., Mössbauer effect in $Mn_xFe_{3-x}O_4$. *J. Phys. Soc. Japan*, **18** (1963) 1091.
16. Kulkarni, J. A. & Darshane, V. S., Effect of high temperature on cation distribution: $NiMn_2O_4$–$FeMn_2O_4$ system. *Thermochim. Acta*, **93** (1985) 473–6.
17. Rousset, A., Legros, R. & Lagrange, A., Recent progress in the fabrication of ceramic negative temperature coefficient thermistors. *J. Eur. Ceram. Soc.*, **3** (1994) 185–95.
18. Singh, V. K., Khatri, N. K. & Lokanathan, S., Mössbauer study of $Co_xMn_{3-x-y}Fe_yO_4$ and $Ni_xMn_{3-x-y}Fe_yO_4$ systems. *Ind. J. Pure & Appl. Phys.*, **20** (1982) 83–9.
19. Castelan, Ph., Contribution à l'étude des propriétés électriques et du phénomène de vieillissement des thermistances C.T.N. à base de manganites à valence mixtes. *Thesis*, University Paul Sabatier, Toulouse, France (1993).
20. Goodenough, J. B. & Loeb, A. L., Theory of ionic ordering crystal distorsion and magnetic exchange due to covalent forces in spinels. *Phys. Rev.*, **98** (1955) 391–408.
21. Driessens, F. C. M., Place and valence of the cations in Mn_3O_4 and some related manganates. *Inorg. Chim. Acta*, **1** (1967) 193–201.
22. Baffier, N. & Huber, M., Etude par diffraction des rayons

X et des neutrons. Des relations entre distribution cationique et distorsion cristalline dans les ferro-manganites spinelles. *J. Phys. Chem. Solids*, **33** (1972) 737–47.
23. Brabers, V. A. M., Infrared spectra of cubic and tetragonal manganese ferrites. *Phys. Stat. Sol.*, **33** (1969) 563–72.
24. Macklen, E. D. *Thermistors.* Electrochemical Publications Limited, Ayr, Scotland, 1979.
25. Dorris, S. E. & Mason, T. O., Electrical properties and cation valencies in Mn_3O_4. *J. Am. Ceram. Soc.*, **71** (1988) 379–85.